



Wavelength-scanning coherent OTDR for dynamic high strain resolution sensing

SASCHA LIEHR,* SVEN MÜNZENBERGER, AND KATERINA KREBBER

Bundesanstalt für Materialforschung und -prüfung (BAM), Unter den Eichen 87, 12205 Berlin, Germany

*sascha.liehr@bam.de

Abstract: Distributed vibration sensing in optical fibers opened entirely new opportunities and penetrated various sectors from security to seismic monitoring. Here, we demonstrate a most simple and robust approach for dynamic strain measurement using wavelength-scanning coherent optical time domain reflectometry (C-OTDR). Our method is based on laser current modulation and Rayleigh backscatter shift correlation. As opposed to common single-wavelength phase demodulation techniques, also the algebraic sign of the strain change is retrieved. This is crucial for the intended applications in structural health monitoring and modal analysis. A linear strain response down to 47.5 pε and strain noise of 100 pε/√Hz is demonstrated for repetition rates in the kHz range. A field application of a vibrating bridge is presented. Our approach provides a cost-effective high-resolution method for structural vibration analysis and geophysical applications.

© 2018 Optical Society of America under the terms of the [OSA Open Access Publishing Agreement](#)

OCIS codes: (060.2370) Fiber optics sensors; (120.4825) Optical time domain reflectometry; (280.1350) Backscattering; (290.5870) Scattering, Rayleigh.

References and links

1. A. H. Hartog, *An Introduction to Distributed Optical Fibre Sensors* (CRC, 2017).
2. M. K. Barnoski and S. M. Jensen, "Fiber waveguides: A novel technique for investigating attenuation characteristics," *Appl. Opt.* **15**(9), 2112–2115 (1976).
3. R. Bernini, A. Minardo, and L. Zeni, "Dynamic strain measurement in optical fibers by stimulated Brillouin scattering," *Opt. Lett.* **34**(17), 2613–2615 (2009).
4. Y. Peled, A. Motil, L. Yaron, and M. Tur, "Slope-assisted fast distributed sensing in optical fibers with arbitrary Brillouin profile," *Opt. Express* **19**(21), 19845–19854 (2011).
5. J. Urricelqui, A. Zornoza, M. Sagues, and A. Loayssa, "Dynamic BOTDA measurements based on Brillouin phase-shift and RF demodulation," *Opt. Express* **20**(24), 26942–26949 (2012).
6. Y. Mizuno, N. Hayashi, H. Fukuda, K. Y. Song, and K. Nakamura, "Ultrahigh-speed distributed Brillouin reflectometry," *Light Sci. Appl.* **5**(12), e16184 (2016).
7. A. Bergman, T. Langer, and M. Tur, "Phase-based, high spatial resolution and distributed, static and dynamic strain sensing using Brillouin dynamic gratings in optical fibers," *Opt. Express* **25**(5), 5376–5388 (2017).
8. S. V. Shatalin, V. N. Treschikov, and A. J. Rogers, "Interferometric optical time-domain reflectometry for distributed optical-fiber sensing," *Appl. Opt.* **37**(24), 5600–5604 (1998).
9. J. C. Juarez, E. W. Maier, K. N. Choi, and H. F. Taylor, "Distributed fiber-optic intrusion sensor system," *J. Lightwave Technol.* **23**(6), 2081–2087 (2005).
10. Z. Qin, T. Zhu, L. Chen, and X. Bao, "High sensitivity distributed vibration sensor based on polarization-maintaining configurations of phase-OTDR," *IEEE Photonics Technol. Lett.* **23**(15), 1091–1093 (2011).
11. Y. Dong, X. Chen, E. Liu, C. Fu, H. Zhang, and Z. Lu, "Quantitative measurement of dynamic nanostrain based on a phase-sensitive optical time domain reflectometer," *Appl. Opt.* **55**(28), 7810–7815 (2016).
12. A. Hartog and K. Kader, "Distributed fiber optic sensor system with improved linearity," U.S. patent US9170149B2 (2012).
13. G. Tu, X. Zhang, Y. Zhang, F. Zhu, L. Xia, and B. Nakarmi, "The development of an Phi-OTDR system for quantitative vibration measurement," *IEEE Photonics Technol. Lett.* **27**(12), 1349–1352 (2015).
14. Z. Wang, L. Zhang, S. Wang, N. Xue, F. Peng, M. Fan, W. Sun, X. Qian, J. Rao, and Y. Rao, "Coherent Phi-OTDR based on I/Q demodulation and homodyne detection," *Opt. Express* **24**(2), 853–858 (2016).
15. J. P. Dakin and C. Lamb, "Distributed fibre optic sensor system," U.S. patent GB 2 222 247A (1990).
16. A. E. Alekseev, V. S. Vdovenko, B. G. Gorshkov, V. T. Potapov, and D. E. Simikin, "A phase-sensitive optical time-domain reflectometer with dual-pulse diverse frequency probe signal," *Laser Phys.* **25**(6), 065101 (2015).
17. Y. Muanenda, S. Faralli, C. J. Oton, and F. Di Pasquale, "Dynamic phase extraction in a modulated double-pulse phi-OTDR sensor using a stable homodyne demodulation in direct detection," *Opt. Express* **26**(2), 687–701 (2018).

18. R. Posey, G. A. Johnson, and S. T. Vohra, "Strain sensing based on coherent Rayleigh scattering in an optical fibre," *Electron. Lett.* **36**(20), 1688–1689 (2000).
 19. A. Masoudi, M. Belal, and T. P. Newson, "A distributed optical fibre dynamic strain sensor based on phase-OTDR," *Meas. Sci. Technol.* **24**(8), 085204 (2013).
 20. A. E. Alekseev, V. S. Vdovenko, B. G. Gorshkov, V. T. Potapov, I. A. Sergachev, and D. E. Simikin, "Phase-sensitive optical coherence reflectometer with differential phase-shift keying of probe pulses," *Quantum Electron.* **44**(10), 965–969 (2014).
 21. Y. Shi, H. Feng, and Z. Zeng, "Phase-sensitive optical time domain reflectometer with dual-wavelength probe pulse," *Int. J. Distrib. Sens. Netw.* **11**(5), 624643 (2015).
 22. A. H. Hartog and L. B. Liokumovich, "Phase sensitive coherent otdr with multi-frequency interrogation," U.S. patent WO2013066654 A1 (2013).
 23. F. Zhu, X. Zhang, L. Xia, Z. Guo, and Y. Zhang, "Active compensation method for light source frequency drifting in Phi-OTDR sensing system," *IEEE Photonics Technol. Lett.* **27**(24), 2523–2526 (2015).
 24. Z. Wang, Z. Pan, Z. Fang, Q. Ye, B. Lu, H. Cai, and R. Qu, "Ultra-broadband phase-sensitive optical time-domain reflectometry with a temporally sequenced multi-frequency source," *Opt. Lett.* **40**(22), 5192–5195 (2015).
 25. D. Iida, K. Toge, and T. Manabe, "Distributed measurement of acoustic vibration location with frequency multiplexed phase-OTDR," *Opt. Fiber Technol.* **36**, 19–25 (2017).
 26. Y. Koyamada, M. Imahama, K. Kubota, and K. Hogari, "Fiber-optic distributed strain and temperature sensing with very high measurand resolution over long range using coherent OTDR," *J. Lightwave Technol.* **27**(9), 1142–1146 (2009).
 27. L. Zhou, F. Wang, X. Wang, Y. Pan, Z. Sun, J. Hua, and X. Zhang, "Distributed strain and vibration sensing system based on phase-sensitive OTDR," *IEEE Photonics Technol. Lett.* **27**(17), 1884–1887 (2015).
 28. M. A. Soto, X. Lu, H. F. Martins, M. Gonzalez-Herraez, and L. Thévenaz, "Distributed phase birefringence measurements based on polarization correlation in phase-sensitive optical time-domain reflectometers," *Opt. Express* **23**(19), 24923–24936 (2015).
 29. J. Pastor-Graells, H. F. Martins, A. Garcia-Ruiz, S. Martin-Lopez, and M. Gonzalez-Herraez, "Single-shot distributed temperature and strain tracking using direct detection phase-sensitive OTDR with chirped pulses," *Opt. Express* **24**(12), 13121–13133 (2016).
 30. S. Liehr, Y. S. Muanenda, S. Münzenberger, and K. Krebber, "Relative change measurement of physical quantities using dual-wavelength coherent OTDR," *Opt. Express* **25**(2), 720–729 (2017).
 31. P. Rohwetter, R. Eisermann, and K. Krebber, "Random quadrature demodulation for direct detection single-pulse Rayleigh C-OTDR," *J. Lightwave Technol.* **34**(19), 4437–4444 (2016).
-

1. Introduction

Distributed optical fiber sensors have found a wide range of usage in various sectors, from structural health monitoring (SHM), power grid monitoring, to geotechnical, environmental or chemical applications. Nonlinear scattering phenomena in silica fibers, such as Raman and Brillouin scattering, are frequently used for static long-distance temperature (Raman) and strain/temperature (Brillouin) sensing applications.

Dynamic and high-resolution strain sensing is achieved by interferometric Rayleigh backscatter approaches. These distributed vibration sensing (DVS) techniques, often also referred to as distributed acoustic sensing (DAS), are typically based on coherent optical time domain reflectometry (C-OTDR) and have experienced dynamic progress and considerable advances during the last few years in both research and industrial application [1]. Whereas incoherent optical sources are used in standard OTDR for distributed backscatter loss measurement and fault detection [2], C-OTDR utilizes a coherent optical source. Probing the fiber with coherent pulses results in interference of the Rayleigh backscattered power from scattering centers (scatterers) that are located within the width of the forward-propagating optical pulse. The fiber practically resembles a distributed multiple-path interferometer. The resulting jagged appearance of C-OTDR backscatter traces is constant for stable fiber conditions. However, minute changes of the temporal separation of the scatterers, for example due to local strain or temperature variations, can be detected as backscattered power variations. The advantages of these interferometric DVS techniques are the high strain sensitivity, the high measurement repetition rate and long distance range. DVS found application in high-resolution vibration detection in the oil and gas industry, security and perimeter monitoring, and geophysical applications [1]. Wider use in civil engineering and SHM sector is a more recent development. The requirement on the measurement repetition rate is generally lower for structural monitoring applications, but the measurement of the

correct strain magnitude as well as the algebraic sign of strain change is generally required. This sign-correct measurement is a prerequisite, for example, for distributed deformation sensing and mode shape analysis of vibrating structures. The strain magnitude including the sign, however, cannot be determined by most of the proposed DVS principles.

The research presented in this paper aims, therefore, at the development of a DVS approach that enables high-resolution measurement of strain changes including the sign of the strain change. The intended applications are geophysical research, general structural monitoring applications, modal parameter analysis and vibration analysis of extended structures, as presented in this paper, for reinforced concrete bridges. The requirement on dynamic bandwidth are therefore relaxed, but high spatial resolution in the order of one meter is essential.

Also Brillouin scattering-based methods have been proposed for dynamic measurement [3–7], but are not an alternative for most of the intended applications. Brillouin approaches enable absolute strain measurement including the sign information. The distance range, strain range and repetition rates are constantly enhanced. The strain resolution, however, is typically orders of magnitude lower than that of interferometric DVS techniques.

The majority of Rayleigh-based DVS principles utilizes single-pulse and single-wavelength direct-detection approaches [8,9] which only allows for vibration detection. Quantitative strain measurement is not possible from differential power change evaluation due to the random scatterer distribution in the fiber and, thus, an unknown strain transfer function. More complex homodyne and heterodyne coherent-detection methods [10] have been proposed, some of which enable quantitative strain change detection [11–14]. Other phase-resolved DVS techniques (phase-OTDR or Φ -OTDR) are, for instance, based on dual-pulse approaches [15–17]. Also cross-multiply phase demodulation techniques [18,19] or phase-shift keyed pulses [20] enable quantitative strain change measurement. Although these above-mentioned phase-resolved techniques are commonly more complex than simple direct-detection approaches, requiring for example narrow linewidth lasers, additional modulators, GHz frequency sources, additional interferometers and stabilization, polarization management, balanced detection, or high-bandwidth detection, they can generally not determine the necessary algebraic sign of the strain change. To obtain this information, it is necessary, as in any interferometer, to analyze additional spectral information (i.e., utilize more than one wavelength).

The use of multiple pulse wavelengths has, for example, been proposed to improve the signal quality in DVS [21], to retrieve phase information and linearize the strain response [22], to compensate for laser frequency drift [23], or to increase the repetition rate for distributed vibration sensing [24,25]. The additional spectral information has, however, not been used to determine the sign of the strain change by these approaches. True quantitative strain change measurement, including the algebraic sign, can be achieved using multiple-wavelength C-OTDR by means of correlation analysis of backscattered power along one of the three scanning parameters: **Laser wavelength** (equivalent: laser frequency ν), **fiber distance** (equivalent: pulse backscatter time), and **time** (trace-to-trace measurement time): Static strain distribution has been obtained in this way by correlation along the pulse **wavelength axis** relative to a reference measurement that has been pre-recorded at equally spaced individual pulse wavelengths using a homodyne C-OTDR [26] and a direct-detection architecture [27]. Also static distributed birefringence change measurement has similarly been conducted by pulse wavelength shift correlation analysis [28]. Dynamic strain tracking has been achieved by probing the fiber with frequency-chirped pulses and correlating backscattered power signals along the **fiber distance axis** [29]. The correlation of backscattered power signals of alternating optical pulse wavelengths along the **trace-to-trace time axis** has recently been demonstrated for dynamic measurement using a direct-detection approach [30].

In this paper, we propose and demonstrate a most simplified, robust and cost-effective direct-detection technique that enables dynamic and quantitative high-resolution measurement of strain changes including the correct sign. Our method is based on periodically measuring backscatter traces at equidistant pulse wavelengths and correlation along the wavelength axis. It is the first time, to the best of our knowledge, that dynamic measurements can be conducted using a wavelength-scanning approach. The technique relies on direct laser current modulation, does not require averaging and can therefore be used for dynamic sensing applications. The required high spatial resolution of one meter can be achieved without restrictions.

In comparison to the chirped pulse technique [29], the repetition rate is lowered by the number of measured pulse wavelengths, but the system complexity is further reduced since no high-bandwidth sampling and photodetection hardware is required. Compared to the correlation along the trace-to-trace time axis of different wavelength pulses [30], the strain resolution is considerably improved.

The article is organized as follows: The proposed method is theoretically described, and signal processing techniques are defined in section 2. The experimental setup is introduced in section 3, and characterization and field test results are presented in section 4.

2. Method

2.1. Rayleigh scattering interferometry and measurement method

The origins of Rayleigh scattering in silica optical fibers are a great number of sub-wavelength dimensional refractive index variations (scatterers) that became frozen into the fiber core during the drawing process. The backscattered power from a singlemode fiber (SMF) can be described by a one-dimensional speckle model as a set of N discrete scatterers that have a uniform statistical position distribution along the fiber distance axis z . The scatterers' individual reflectivities r , with respect to the incident optical power, can also be modeled by a statistically independent uniform distribution.

The fiber under test (FUT) is periodically probed by rectangular optical pulses with the peak power I_0 and pulse duration τ_d . The pulses are assumed to be monochromatic and linearly polarized, and periodically enter the fiber at the time $t_z = 0$. In addition to this pulse propagation time axis t_z (or fiber distance axis), a second time axis t is introduced to describe the changes of the backscattered power over progressing measurement time (from pulse to pulse). The optical power $I(t, t_z)$, as detected by a square-law photodetector, from forward-propagating optical pulses corresponds to the time-averaged and squared absolute values of the sum of the discrete backscattered optical field components. The total detected power is composed of a direct summation power component $I_d(t_z)$ and a coherent summation component $I_{coh}(t, t_z)$ as

$$\begin{aligned} I(t, t_z) &= \left| \sum_{i=1}^N \sqrt{r_i} \hat{E}_0 e^{j2\pi\nu_0(t_z - \tau_i(t))} \text{rect}\left(\frac{t_z - \tau_i(t)}{\tau_d}\right) \right|^2 \\ &= I_d(t_z) + I_{coh}(t, t_z) = \sum_{i=1}^N r_i I_0 \text{rect}\left(\frac{t_z - \tau_i}{\tau_d}\right) + I_{coh}(t, t_z) \end{aligned} \quad (1)$$

with \hat{E}_0 and ν_0 being the amplitude and frequency of the optical field. The return time delay of the backscatter signal of the i th scatterer is described by $\tau_i = 2n_g z_i / c_0$, where z_i are the positions of the scatterers along the fiber, c_0 is the vacuum speed of light, and n_g is the effective group refractive index of the fiber. Rectangular-shaped pulse propagation is assumed as $\text{rect}\{[t_z - \tau_i(t)]/\tau_d\} = 1$ for $0 \leq \{[t_z - \tau_i(t)]/\tau_d\} \leq 1$, and 0 otherwise. Only scatterers within the fiber section occupied by half the width w of the propagating pulse in the fiber, with $w/2 = c_0 \tau_d / (2n_g)$, contribute to the detected power, which effectively defines the two-point spatial

resolution $w/2$ of the sensor system ($\tau_d = 10$ ns corresponds to about 1 m spatial resolution). Whereas the direct summation component $I_d(t_z)$ can be approximated to be independent from relative scatterer displacements over the progressing time t , the coherent power component $I_{coh}(t, t_z)$ is sensitive to any temporal delay change between scatterers, for example due to local strain or temperature variations. $I_{coh}(t, t_z)$ can be described by a double summation of all scatterers' phase relations as

$$I_{coh}(t, t_z) = \sum_{i=2}^N \sum_{e=1}^{i-1} 2\sqrt{r_i r_e} I_0 \cos[2\pi\nu_0 \tau_{ie}(t)] \text{rect}\left[\frac{t_z - \tau_i(t)}{\tau_d}\right] \text{rect}\left[\frac{t_z - \tau_e(t)}{\tau_d}\right] \quad (2)$$

with $\tau_{ie} = \tau_i - \tau_e = 2n_g z_{ie} / c_0$ as the scatterers' relative delays and $z_{ie} = z_i - z_e$ being the physical separation between the individual scatterers. Propagation loss along the fiber is neglected and polarization preservation within $w/2$ is assumed. The phase term $\cos[2\pi\nu_0 \tau_{ie}(t)]$ determines the local interferometric power variations and contains τ_{ie} and ν_0 as factors. Any physical change occurring along the fiber may have an impact on the temporal delays. This is typically due to strain or temperature variations, but also other refractive index-altering or birefringence-altering effects may have a marginal influence. Temperature variations ΔT and strain changes $\Delta\varepsilon = \Delta z_{ie} / z_{ie}$ are the most common measurands and can be approximated to have a linear impact on temporal scatterer delay changes $\Delta\tau_{ie}$. The delay change relation $\Delta\tau_{ie} / \tau_{ie}$ can be equivalently correlated to the pulse-to-pulse relative optical frequency change relation $\Delta\nu_p / \nu_0$ by means of the strain coefficient $K_\varepsilon \approx -0.78$ and temperature coefficient $K_T \approx -6.92 \times 10^{-6}$ [26] for SMF as

$$\begin{aligned} \frac{\Delta\nu_p}{\nu_0} &= -\frac{\Delta\tau_{ie}}{\tau_{ie}} = -(1 - p_e)\Delta\varepsilon = K_\varepsilon \Delta\varepsilon \approx -0.78\Delta\varepsilon \\ \frac{\Delta\nu_p}{\nu_0} &= -\frac{\Delta\tau_{ie}}{\tau_{ie}} = -(\xi + \alpha)\Delta T = K_T \Delta T \approx -6.92 \times 10^{-6} \Delta T \end{aligned} \quad (3)$$

where $p_e \approx 0.22$ is the effective strain-optic coefficient of silica, ξ is the thermo-optic coefficient of silica and α is the thermal expansion coefficient of the fiber. Negligible proportionality deviation can be assumed under realistic application scenarios with $|\Delta\tau_{ie} / \tau_{ie}| \ll 1$ and $|\Delta\nu_p / \nu_0| \ll 1$. Optical delay changes $\Delta\tau_{ie}(t)$ relative to the initial scatterer delays τ_{ie} over the progressing measurement time t can be described as a superposition of occurring strain changes $\Delta\varepsilon(t, t_z)$ and temperature changes $\Delta T(t, t_z)$ along the fiber distance axis (function of t_z). The delay changes can therefore be substituted as

$$\tau_{ie} - \Delta\tau_{ie}(t) = \tau_{ie} \left[1 + K_\varepsilon \Delta\varepsilon(t, t_z) + K_T \Delta T(t, t_z) \right] \quad (4)$$

This equation may be further expanded by other delay-proportional impact parameters. It is evident from Eq. (3) that changes of the optical frequency $\Delta\nu_p$ have an equivalent impact on delay changes $\Delta\tau_{ie}$. Substituting delays from Eq. (4) by frequency changes leads to a total detected backscatter power dependence of

$$\begin{aligned} I(t, t_z, \Delta\nu_p) &= I_d(t_z) + \sum_{i=2}^N \sum_{e=1}^{i-1} 2\sqrt{r_i r_e} I_0 \cos\left\{ 2\pi(\nu_0 + \Delta\nu_p) \tau_{ie} \left[1 + K_\varepsilon \Delta\varepsilon(t, t_z) + K_T \Delta T(t, t_z) \right] \right\} \\ &\quad \times \text{rect}\left[\frac{t_z - \tau_i(t)}{\tau_d}\right] \text{rect}\left[\frac{t_z - \tau_e(t)}{\tau_d}\right] \end{aligned} \quad (5)$$

Equation (5) shows that optical frequency changes $\Delta\nu_p$ and strain/temperature changes $\Delta\varepsilon$ and ΔT are interchangeable factors in the phase term. Changes of temperature and strain can therefore be compensated by equivalent pulse optical frequency changes $\Delta\nu_p$. The compensation is total under the condition that ΔT and $\Delta\varepsilon$ are uniform within $w/2$. The absolute scatterer position changes $\tau_i(t)$ and $\tau_e(t)$ can be neglected for most applications but

will have a degrading effect on the correlation quality if they are greatly shifted with respect to the pulse sampling positions.

2.2 Wavelength-scanning approach

Correlation of backscattered power signatures from multiple wavelength pulses has been demonstrated along the three parameters: t , t_z and Δv_p . The correlation along the trace-to-trace time axis t between two different pulse wavelength groups has been proposed for strain and temperature measurement [30]. A correlation approach along the fiber distance axis t_z has been demonstrated using linearly chirped pulses [29]. The aim of our proposed measurement technique, however, is to correlate along the frequency (or wavelength) shift axis Δv_p . Similar to [26] for static sensing, we determine strain and temperature changes by measuring corresponding optical frequency shifts. Backscattered power signals are measured over a range of discrete pulse optical frequency values and the shift is determined by some kind of correlation analysis. Our approach, however, aims at dynamic measurement at increased strain resolution utilizing a most simplified and robust hardware implementation. Therefore, the pulse optical frequency is periodically and linearly tuned during consecutive backscatter measurements with the pulse repetition period τ_p (pulse repetition frequency $f_p = 1/\tau_p$). The laser frequency sweep is achieved by simple direct modulation of the laser current with a saw-tooth signal, as depicted in Fig. 1.

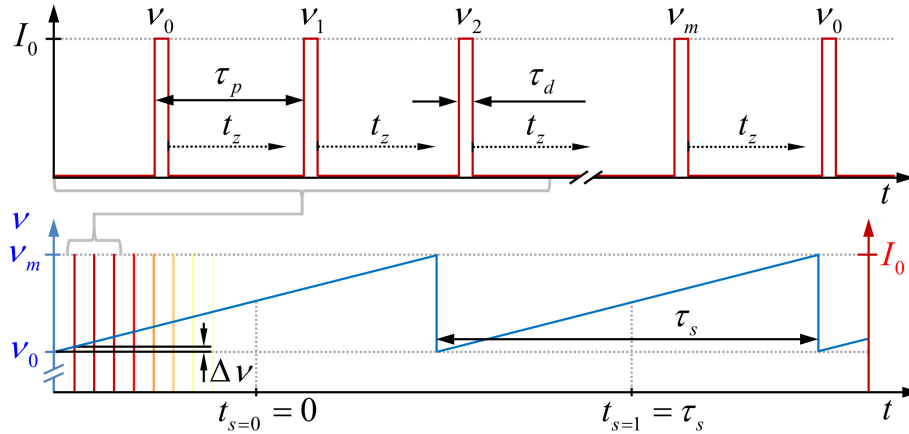


Fig. 1. Schematic of the pulse generation and frequency sweep approach.

The optical frequencies of the pulses are defined as $v_p = v_0 + \Delta v_p$ with discrete frequency steps of Δv with $\Delta v_p = p\Delta v$, and $p = 0, 1, 2, \dots, m$. Backscatter traces of $m + 1$ pulse optical frequency values are measured during the laser sweep period τ_s (integer multiple of τ_p). The frequency shift-equivalent strain or temperature change values, $\Delta\varepsilon(t, t_z)$ and $\Delta T(t, t_z)$, are obtained by correlation analysis of $I(t, t_z, \Delta v_p)$ along the Δv_p axis for each fiber position $z = t_z c_0 / (2n_g)$. The correlation is conducted for the effective sweep sampling times $t = t_s = n\tau_s$, with $n \in \mathbb{N}_0$ (as indicated in Fig. 1), and relative to a reference sampling time $t = t_{ref}$. The effective measurement repetition rate is $f_s = 1/\tau_s$. The pulse-to-pulse backscatter variations for 1000 frequency sweeps $I(t_s, \Delta v_p)$ for one sensor position z (one random set of N scatterers) are simulated in Fig. 2(a). A 10 Hz harmonic strain signal $\Delta\varepsilon(t_s)$ with a peak amplitude of $1 \mu\varepsilon$ (strain units are given in ε , with $1 \varepsilon \hat{=} 1 \text{ m/m}$) is superimposed using Eq. (5). The strain-equivalent frequency shift proportionality is evident in Fig. 2(b).

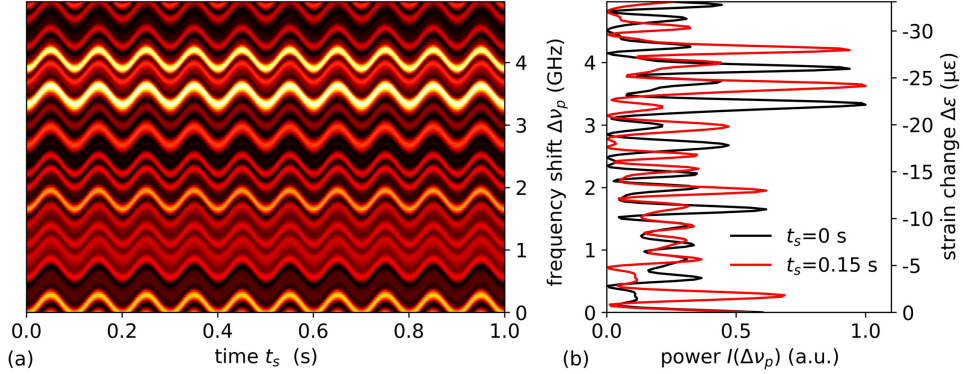


Fig. 2. (a) Simulated power results $I(t_s, \Delta v_p)$ during a sinusoidal strain signal of $1 \mu\epsilon$ peak amplitude for one fiber position z and a set of $N = 1000$ scatterers ($f_s = 1 \text{ kHz}$, $f_p = 200 \text{ kHz}$, $\tau_d = 6 \text{ ns}$, $\Delta v_p = 5 \text{ GHz}$, $\Delta v = 25 \text{ MHz}$). (b) Strain-equivalent power shift of $I(\Delta v_p)$ for the sweep times $t_s = 0 \text{ s}$ and $t_s = 0.15 \text{ s}$ ($\Delta\epsilon = 2 \mu\epsilon$).

2.3 Correlation and interpolation approach

We propose a least square correlation algorithm to determine the strain or temperature change-equivalent measured frequency shift Δv_m relative to a reference time t_{ref} by determining the minimum argument of the correlation result $R_{ref,s}(q)$ as

$$\Delta v_m(t_s, t_z) = \arg \min_q [R_{ref,s}(q)] \Delta v \quad (6)$$

with

$$R_{ref,s}(q) = \begin{cases} \frac{1}{m-q} \sum_{p=0}^{m-q} [I(t_{ref}, t_z, \Delta v_{p+q}) - I(t_s, t_z, \Delta v_p)]^2 & q \geq 0 \\ R_{s,ref}(-q) & q < 0 \end{cases} \quad (7)$$

and $|q| < m$. This least square correlation algorithm shows improved stability and performance regarding faulty correlation results and precision in comparison to standard cross correlation analysis. The proposed algorithm also exhibits comparable results to Pearson's correlation coefficient analysis, used in [26,27], but at considerably reduced computational expense.

The measurable strain range depends on the number of pulse frequencies and the used frequency sweep range Δv_p . It is roughly equivalent to $\pm \Delta v_p/4$ for error-free correlation with a single, fixed reference sweep result $I(t_{ref}, t_z, \Delta v_p)$. For comparison, a frequency shift of 1 GHz corresponds to a strain change of about $-6.7 \mu\epsilon$. In section 4.2, however, we propose a method that allows for continuously expanding the measurable strain range beyond this frequency sweep range limitation. Another possibility to extend the strain range is to conduct a sweep-to-sweep correlation (each sweep result correlated with the previous sweep result), similar to [29,30], and obtain the strain change $\Delta\epsilon(t_s)$ from accumulative summation of the consecutive shift results. This technique, however, results in accumulated strain error and degradation of the low-frequency strain response if the errors are not appropriately handled.

The sampling resolution of the measured frequency shift Δv_m is effectively increased by more than two orders of magnitude beyond the frequency step size Δv by interpolation of $R_{ref,s}(q)$. The argmin operation of the cubic polynomial interpolation result $R'_{ref,s}(q')$ with an interpolation factor k_p ($k_p = \Delta v/\Delta v'$) yields the high sampling resolution of the measured frequency shift. This effectively upsampled shift result Δv_m is used throughout this paper with an interpolation factor of $k_p = 500$. An example $R_{ref,s}(q)$ and $R'_{ref,s}(q')$ is shown in Fig. 5(d).

For a correct minimum interpolation of $R'_{ref,s}(q')$ and, hence, a linear strain response, it is important that the widths of the $R_{ref,s}(q)$ minima are several samples wide. This implies that

the average feature widths of $I(\Delta\nu_p)$ are several samples wide; compare Fig. 3(b) and Fig. 5(c),(d). This can be ensured and optimized by taking physically substantiated scattering statistics into account. Since the mean periodicity and also the mean width of the backscatter peaks of $I(\Delta\nu_p)$ is statistically determined by the mean scatterer delays τ_{ie} within $w/2$ [31], an appropriate value of the frequency step $\Delta\nu$ for a given pulse duration τ_d can be chosen to satisfy this requirement. The theoretical maximum feature periodicity of $I(\Delta\nu_p)$ is limited by the maximum scatterer delays τ_{ie} . We determined a practical value for the relation coefficient $g = \Delta\nu \tau_d$ to be in the order of $g \approx 0.25$ for rectangular pulses. This way, the repetition rate and frequency scan range can be maximized for a given pulse duration τ_d . The linearity and sensitivity of the strain- $\Delta\nu_m$ transfer for sub- $\Delta\nu$ strain amplitudes and the applicability of this correlation and interpolation approach is demonstrated in section 4.

2.4 Laser sweep linearization

The frequency chirp during the pulse duration τ_d for most measurements in this paper is in the order of 20 kHz and can be neglected. The frequency change during τ_s , however, is not entirely linear for the experimentally implemented direct laser current modulation and has to be compensated by numerical linearization. This is especially important for higher strain values, and when widely shifted sweep sequences have to be correlated. Figure 3(a) shows the frequency change during τ_s that has experimentally been determined from a phase change measurement in an unbalanced Mach-Zehnder interferometer.

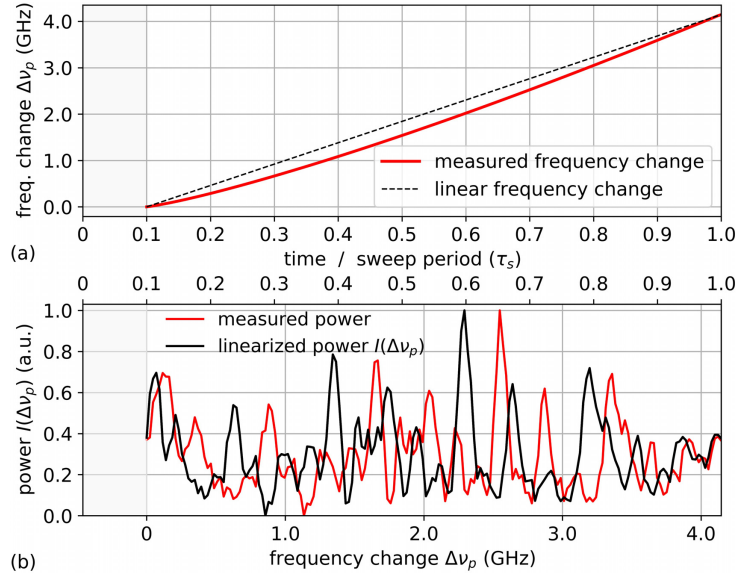


Fig. 3. (a) Measured frequency change $\Delta\nu_p$ relative to ν_0 during the laser current modulation, obtained from phase change analysis in an unbalanced Mach-Zehnder interferometer ($f_s = 1$ kHz, $f_p = 200$ kHz, $\tau_d = 10$ ns, $\Delta\nu_p = 4.15$ GHz, $\Delta\nu = 23.07$ MHz). (b) Measured and numerically linearized $I(\Delta\nu_p)$ during the sweep period τ_s .

The section in the beginning of the saw-tooth sweep segment ($< \tau_s / 10$) is not used for the correlation sequence due to the negative frequency slope after the falling edge of the saw-tooth current modulation signal. Figure 3(b) shows the directly measured backscatter power during the frequency sweep, and the numerically linearized power $I(\Delta\nu_p)$ which is eventually used for the correlation analysis using Eq. (7).

The strain distributions are calculated from $\Delta\nu_m(t_s, t_z)$ and the interpolated $R'_{ref,s}(q')$ correlation results with the numerically linearized sweep sequences $I(t_s, t_z, \Delta\nu_p)$ as input vectors for each sampling time t_s and each position t_z as

$$\Delta\varepsilon(t_s, t_z) = \frac{\Delta v_m(t_s, t_z)}{K_\varepsilon v_0} \quad (8)$$

The experimental implementation of these methods is presented in the following section. Performance and application tests for distributed strain measurement are summarized in section 4.

3. Experimental setup

The aim of the proposed correlation approach and experimental implementation was to realize a robust, high-resolution DVS system with the focus on a simple design and low-cost components. A single channel direct-detection architecture has been implemented. The schematic of the experimental setup of the technique is depicted in Fig. 4.

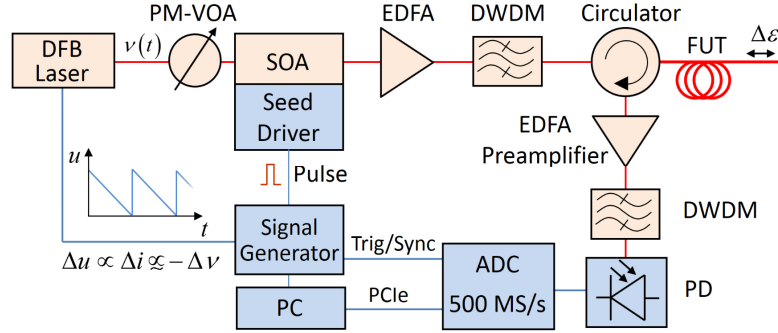


Fig. 4. Schematic of the wavelength-scanning coherent OTDR implementation.

A low-cost distributed feedback (DFB) laser diode with a spectral width of 1.3 MHz and a center wavelength of 1549.89 nm ($v_0 \approx 193.36$ THz) is used in continuous wave (CW) mode. The coherence length in the fiber is in the order of 50 m. The degree of coherence loss within the pulse length can therefore be neglected for pulse widths of a few meters. The central component is a 120 MHz two-channel signal generator, which supplies the synchronized sawtooth voltage signal Δu for the laser current modulation Δi and, consequently, the frequency modulation Δv ($\Delta v/\Delta u \approx -20$ MHz/mV). It also supplies the rectangular signal for the pulse shaping as well as the trigger and synchronization signal for the data acquisition. The optical pulses are generated by a semiconductor optical amplifier (SOA) which is operated via a seed driver as a fast optical switch with a high nominal extinction ratio of 70 dB. Deviations of the laser spectral properties due to SOA pulse shaping were not observed. The SOA CW input power is adjusted by a polarization-maintaining variable optical attenuator (PM-VOA). The optical pulse signal is subsequently amplified to several hundred mW peak power I_0 by an erbium-doped fiber amplifier (EDFA) in constant-current mode. Amplified spontaneous emission (ASE) noise is filtered out by a low-cost telecom-grade dense wavelength-division multiplexing (DWDM) filter (0.2 nm bandwidth, flat-top) before the pulse signal is coupled into the standard singlemode FUT via a polarization-insensitive optical circulator. All backscattered power is amplified by an EDFA pre-amplifier in constant-current mode and is subsequently ASE-filtered by a second DWDM filter. The optical backscatter power signal is converted to the electrical domain by a 125 MHz bandwidth PIN photodetector (PD) with an integrated transimpedance gain. The backscatter signal, triggered by the signal generator, is sampled with a 14-bit resolution by a 500 MS/s analog-to-digital converter (ADC). The sampling period translates to a spatial sampling resolution of about 20.4 cm. That means that, at spatial resolutions in the meter-range, the adjacent backscatter sampling points comprise a considerable overlap of the axial strain distribution as well as the Rayleigh scatterer contribution.

An accuracy-limiting factor for long-term and quasi-static strain or temperature measurement is the frequency stability of the laser source. The calculated maximum strain and temperature deviation due to temperature controller drift in combination with the DFB laser over 24 hours is equivalent to $\Delta\epsilon \approx \pm 120$ ne and $\Delta T \approx \pm 13.4$ mK, respectively. The reason for the non-symmetric saw-tooth laser current modulation signal (as opposed to using a symmetric triangular modulation or the linear slope of a sine signal) is to determine the phase of the sweep modulation. This is achieved at the beginning of the measurement by a trace-to-trace discontinuity analysis of the backscatter signal to identify the falling slope. The motivation is to maintain maximum system simplicity and avoid the need for a second data acquisition channel just for laser sweep phase recovery.

The maximum pulse repetition rate is limited by the fiber length z_{max} with $f_{p,max} = c_0/(2n_g z_{max})$. The maximum measurement repetition rate for the wavelength-scanning mode, however, is reduced to f_s by the number of pulse frequency steps. Repetition rates in wavelength-scanning mode can be in the kHz range for fiber lengths of a few kilometers, which is more than sufficient for vibration analysis of extended structures and general health monitoring applications. The frequency range also covers the required bandwidth for seismic measurement (5-150 Hz) [1]. The measurement mode of the setup can also be instantly changed to single-wavelength differential power change analysis with fiber length-limited repetition rates up to $f_s = 7$ MHz. Alternatively, measurement of higher strain rates, but lower strain resolution and lower repetition rate, can be conducted with this setup by using the dual-wavelength correlation approach from reference [30] and correlating power signatures along the time axis.

The measurement repetition rate could be increased by probing the FUT with pulses of different wavelength in parallel. The frequency demodulation, however, would result in an unacceptable increase of hardware demand for optical filtering and frequency-diverse detection. Frequency demodulation in the signal domain using short Fourier transform analysis [25] requires longer pulse durations, which is not acceptable for the high spatial resolution requirements of most SHM applications.

4. Results

4.1 Performance characterization

The performance of the proposed sensor system is ultimately determined by the validity of the theoretical assumptions made in section 2. This includes, for example, the physical and numerical implementation of the sweep linearization, the linearity of the strain- Δv_m transfer for interpolated results $R'_{ref,s}(q')$, as well as the overall reliability and stability of the correlation algorithm. This is particularly important for fiber sections where strong non-homogenous strain distributions occur within the spatial resolution $w/2$, and the similarity of $I(t_{ref}, \Delta v_p)$ and $I(t_s, \Delta v_p)$ is thus effectively distorted.

The performance has initially been tested and quantified under controlled laboratory conditions. A 970 m long FUT has been placed in a vibration-damped and temperature-stabilized box. A 14 m long fiber section at the fiber end (about 936.5 m to 950.5 m) has been wound around a piezo tube. The piezo is used to apply harmonic strain signals to the fiber with amplitudes from the pe-range up to several $\mu\epsilon$. As an example, Fig. 5(a) displays the temporal strain distribution for this fiber section during a 20 Hz and 97 ne peak amplitude excitation. Figure 5(b) shows the strain result for a single sensor position at $z = 942.11$ m. The raw backscattering power results at $z = 942.11$ m are shown in Fig. 5(c) and the corresponding correlation results are depicted in Fig. 5(d). The 3D depiction of a 120 Hz and 97 ne peak amplitude signal in Fig. 5(e) displays the strain amplitude spectral density (ASD) calculated from one second recorded $I(t_s, t_z, \Delta v_p)$ results. The strain response of the piezo tube has been confirmed by Mach-Zehnder reference measurement. These results demonstrate that

the correlation technique is very robust, even at the edges of the strained fiber section where strong inhomogeneous strain distributions within the spatial resolution cells occur.

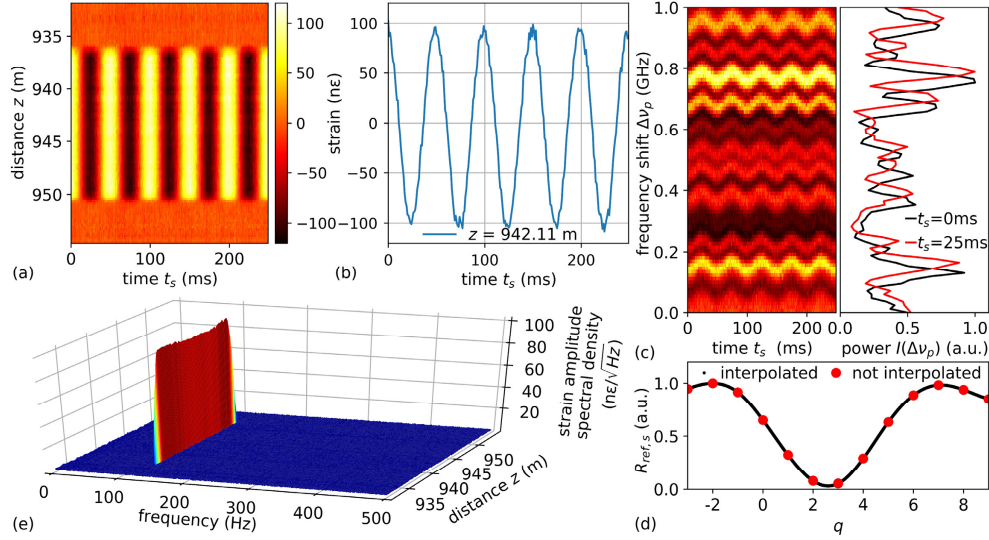


Fig. 5. (a) Temporal strain distribution of a strained fiber section (97 nε peak amplitude at 20 Hz) from $z = 936.5$ m to $z = 950.5$ m. (b) Strain for a single sensor position during the same measurement at $z = 942.11$ m. (c) Measured raw data for strain results in (a) and (b): backscattering power $I(\Delta\nu_p)$ at the position $z = 942.11$ m for 250 frequency sweeps (left) and two single sweep results $I(\Delta\nu_p)$ at the sweep times $t_s = 0$ ms and $t_s = 25$ ms (right). The y-axis refers to both subplots of (c). (d) Correlation result $R_{ref,s}(q)$ and interpolated result $R'_{ref,s}(q')$ of the sweep measurements shown in the right panel of (c). (e) Strain amplitude spectral density plot for a 120 Hz signal with 97 nε amplitude (one second measurement time). The strain amplitudes of the fiber region wound in the center of the piezo tube exhibit slightly reduced strain amplitudes due to the non-uniform diameter change of the piezo tube. Parameters for all measurements in Fig. 5: $f_s = 1$ kHz, $f_p = 100$ kHz, $\tau_p = 20$ ns, $\Delta\nu_p = 1.01$ GHz, $\Delta\nu = 11.94$ MHz

The spatial separation between unstrained fiber sections and full strain amplitudes in Fig. 5(a),(e) is less than the nominal spatial resolution of 2 m. The high harmonic suppression also proves the linearity of the strain- $\Delta\nu_m$ transfer at the uniformly and, more importantly, at not uniformly strained sensor resolution cells. Figure 6 displays the strain ASD and strain amplitude responses in logarithmic scale for two sensor locations at strained and unstrained fiber sections, respectively.

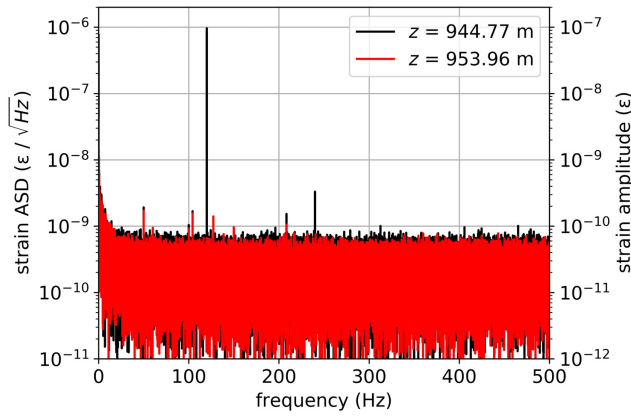


Fig. 6. Strain amplitude spectral density and strain amplitude at positions with ($z = 944.77$ m) strain modulation and without ($z = 953.96$ m) strain modulation ($f_s = 1$ kHz, $f_p = 100$ kHz, $\tau_d = 20$ ns, $\Delta\nu_p = 1.01$ GHz, $\Delta\nu = 11.94$ MHz, 100 s measurement time).

This result demonstrates the high linearity (low harmonic distortion) of the physical implementation as well as the validity of the numerical operations introduced in section 2. The suppression of the second harmonic is in the order of 25 dB (corresponding to 50 dB in the often-used power spectral density characterization in this field). The visible strain amplitudes at 50 Hz and 104 Hz (and harmonics thereof) in the order of 50-170 $\mu\epsilon$ are presumably due to electrical oscillations directly affecting the laser current stability. They could, however, be spectrally removed since they are constant in amplitude and coherent in phase. The reliability of the method to correctly measure distributed perturbations at multiple positions along the fiber is demonstrated for a measurement application in section 4.

The strain resolution is characterized by the minimum detectable strain amplitude at the presence noise. This is best described independent of the dynamic bandwidth of the system by the strain amplitude spectral density noise in $\text{n}\epsilon/\sqrt{\text{Hz}}$. The strain ASD noise for the measurement above is about 0.23 $\text{n}\epsilon/\sqrt{\text{Hz}}$, and approximately white noise for $f > 10$ Hz. The temperature noise corresponds to 26 $\mu\text{K}/\sqrt{\text{Hz}}$. The strain ASD noise for the field application in Fig. 9 at 1 m spatial resolution ($\tau_d = 10$ ns, $f_s = 1$ kHz, $z_{\max} \approx 510$ m) is about 0.30 $\text{n}\epsilon/\sqrt{\text{Hz}}$. The ASD noise for various spatial resolutions settings and distance ranges at $f_s = 1$ kHz is listed as an example in Table 1.

Table 1. Strain ASD noise in $\text{n}\epsilon/\sqrt{\text{Hz}}$ at $f_s = 1$ kHz for various nominal spatial resolutions (0.5 m to 5 m) and distance ranges z_{\max}

Pulse duration τ_d	$z_{\max} \approx 1020$ m	$z_{\max} \approx 2040$ m
5 ns	2.30	2.54
10 ns	0.50	0.69
20 ns	0.23	0.34
50 ns	0.16	0.20

Higher resolution can be achieved by using longer pulse durations τ_d at the cost of spatial resolution, or by tuning τ_s and τ_p towards reduced repetition rates or reduced distance ranges. Analogously, the repetition rate and/or the distance range can be increased for adjusted measurement parameters at lower strain resolutions. Strain resolutions of 0.10 $\text{n}\epsilon/\sqrt{\text{Hz}}$ can, for example, be reached for $f_s = 2$ kHz, $\tau_d = 50$ ns and $z_{\max} \approx 510$ m.

As addressed in section 2.3, the validity of the interpolated $R'_{ref,s}(q')$ results for sub- Δv -equivalent strain resolution is an important issue. The linearity of the strain response is confirmed by analyzing the strain amplitudes over a wide strain amplitude range and well below the Δv -equivalent strain quantization limit. Figure 7 shows the measured strain amplitudes for a wide range of harmonic 120 Hz piezo voltages.

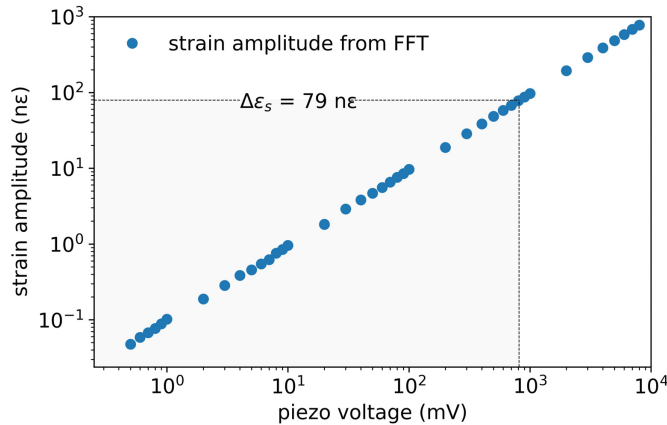


Fig. 7. Measured strain peak amplitudes from spectral strain amplitude analysis as a function of piezo modulation voltage. $\Delta\epsilon_s \approx 79$ $\text{n}\epsilon$ indicates the equivalent measurement frequency step size of $\Delta v \approx 11.94$ MHz. ($f_s = 1$ kHz, $f_p = 100$ kHz, $\tau_d = 20$ ns, $\Delta v_p = 1.01$ GHz).

The strain response is linear over more than four orders of magnitude from of 47.5 $\mu\epsilon$ amplitude to 778 $\mu\epsilon$, and more than three orders of magnitude below the Δv -equivalent strain value $\Delta\epsilon_s = 79 \text{ n}\epsilon$ for the settings $\Delta v\tau_d \approx 0.24$. This confirms the applicability of the interpolation approach and demonstrates that the system can be used for distributed vibration quantification in the $\mu\epsilon$ range.

4.2 Dynamic strain range expansion

The advantage of scanning and correlation along the frequency shift axis is the undistorted $I(\Delta v_p)$ dependence on strain, as evident from Eq. (5). Only signal shifts occur for uniform strain distributions. That ensures long-term stable measurement over a wider strain range due to the comparison with a highly correlated reference. The undistorted $I(t_s, \Delta v_p)$ shift as a function of strain has another beneficial implication: Although the measurable strain range is methodically restricted by the frequency shift envelope of the laser sweep Δv_p , this limitation can be broken by using the backscattered power data of strain-shifted new sweep results $I(t_s, \Delta v_p)$ that exceed the Δv_p limit after the correlation. This new data is used to continuously expand the power reference $I(t_{ref}, \Delta v_p')$ beyond Δv_p by appending the new power results that exceed the Δv_p range. An example of a measurement $I(t_s, \Delta v_p)$ during an amplitude-modulated harmonic strain excitation is shown in Fig. 8(a). The continuously expanding reference spectrum $I(t_{ref}, \Delta v_p')$ from this measurement is depicted in Fig. 8(b). The measured strain result, obtained from correlation with $I(t_{ref}, \Delta v_p')$, is plotted in Fig. 8(c).

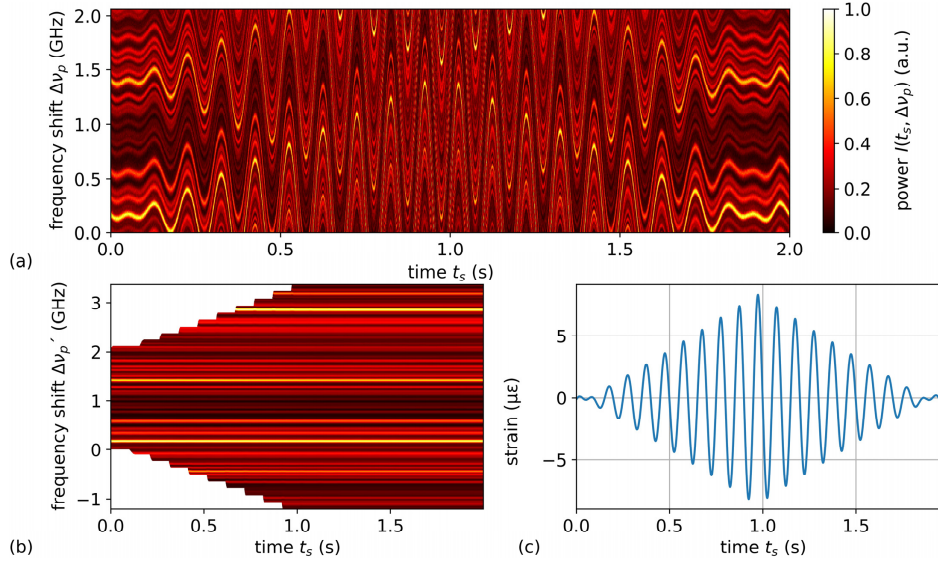


Fig. 8. (a) Measured $I(t_s, \Delta v_p)$ of an amplitude modulated 10 Hz harmonic strain signal for one fiber position ($f_s = 1 \text{ kHz}$, $f_p = 200 \text{ kHz}$, $\tau_d = 10 \text{ ns}$, $\Delta v_p = 2.06 \text{ GHz}$, $\Delta v = 11.84 \text{ MHz}$). (b) Continuously extending reference $I(t_{ref}, \Delta v_p')$ over time as the strain amplitude exceeds the boundaries of Δv_p . (c) Measured strain result from correlation with $I(t_{ref}, \Delta v_p')$.

Extending the reference to $I(t_{ref}, \Delta v_p')$ does not only break the boundaries of the strain measurement range, but also improves the correlation results due to a wider correlation reference range. The strain range during a continuous measurement is only limited by the physical strain range of the fiber. No tunable laser source, tunable filters or external high-bandwidth modulation is required to cover the continuous range expansion. The only restriction is the maximum strain rate that still ensures partially overlapping sweep results for correct correlation and allows for continuous reference patching.

By storing the extended reference spectrum, it is also possible to resume an interrupted measurement and conduct relative strain change measurements at irregular intervals. Since

the backscattered power signature as a function of $\Delta\nu$ is distinct and non-periodic, the correlation of resumed sweep results with $I(l_{ref}, l_z, \Delta\nu_p)$ yields correct and unambiguous shift results. This functionality is very useful for long-term monitoring applications, where additional absolute strain change information is required. Temporarily interrupted strain change measurement is also achieved by the static approach in [26], but is generally not feasible for dynamic phase-demodulation DVS methods.

4.3 Field application

The experimental setup has been tested in an actual structural monitoring application. A 24.4 m long two-span reinforced concrete bridge model has been constructed for the purpose of structural and modal vibration analysis. For the analysis of modal parameters, it is crucial to not only determine the precise strain distribution, but also the sign of the strain change.

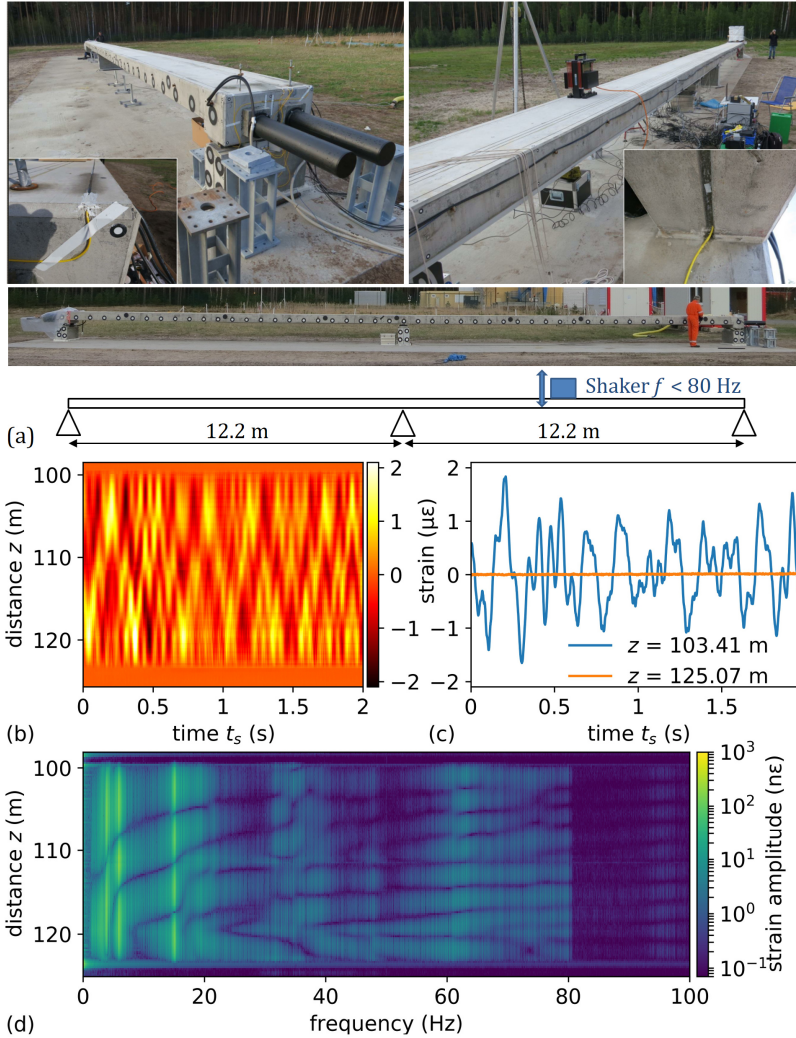


Fig. 9. (a) Images and schematic of the bridge model with applied sensor fiber and shaker. (b) Measured strain distribution along the length of the bridge during the shaker excitation ($<math><math>f < 80\text{ Hz}</math></math> with a white noise signal ($f_c = 1$ kHz, $f_p = 200$ kHz, $\tau_d = 10$ ns, $\Delta\nu_p = 4.15$ GHz, $\Delta\nu = 23.07$ MHz). (c) Measured strain at two fiber locations: In the middle of one span and after the bridge. (d) Strain amplitude spectrum along the bridge indicating the mode shapes and modal frequencies of the structure (from 50 s measurement). The broad spectral content at 123.5 m is due to temperature and strain drifts at an exposed and not surface-bonded section of the fiber.$

The single beam and two-span bridge (12.2 m span lengths) has been instrumented with standard SMF; see Fig. 9(a). The fibers have been glued onto the top and bottom of bridge (twice each) along the entire length of the structure. Fiber sections of a few meters length between the surface-glued sensor sections are installed in strain-free condition. The strain distribution has been measured with $f_s = 1$ kHz repetition rate and 1 m nominal spatial resolution ($\tau_d = 10$ ns) during a white noise (< 80 Hz) vibrational excitation with a shaker placed on top of the bridge at not centered position between two supports. The measured strain distribution along the 24.4 m length of the two spans is shown for two seconds in Fig. 9(b). The two deflected spans of the bridge can be clearly identified. More information of the structural response is revealed when the strain amplitudes are displayed in the Fourier domain, as depicted in Fig. 9(d). The individual mode shapes and the respective modal frequencies are clearly visible. Due to the white noise excitation of the vibration, the modes are blurred, but the transitions between different vibrational modes can be analyzed. The darker, horizontally running lines of lower strain amplitudes in Fig. 9(d) represent the nodes of various vibration modes and the transition between the different mode shapes. The distinct vertical lines, for example at 3.8 Hz, 5.9 Hz and 15.2 Hz, are the first three allowed bending modes of the structure. Their frequencies have been numerically predicted and have been confirmed also by accelerometer measurements. The nominal spatial resolution of 1 m enables the separation and identification of higher modes of vibration with smaller spatial extension, as the 2.4 m modes at around 95 Hz. Their amplitudes in the range of 100 pε are visible and can be spectrally and spatially analyzed. The optical fiber-based high-resolution distributed analysis of vibrating structures is a powerful new tool for the structural monitoring and damage assessment of infrastructure. The distributed analysis of mode shape changes and mode frequency changes can be used for early damage assessment.

5. Conclusion

In this work, we demonstrated, to our knowledge for the first time, a wavelength-scanning coherent OTDR approach for dynamic strain change measurement. The spectral backscatter analysis makes it possible to determine the algebraic sign of the strain change which is crucial for a wide range of sensing applications. The technique features a simple, robust and cost-effective architecture and realizes the wavelength-scanning by direct laser current modulation. In contrast to other phase-resolved approaches, no highly coherent sources, polarization management, tunable lasers and filters, interferometer stabilization, high-frequency signal generation or high-bandwidth detection are required.

Numerical sweep linearization and a robust and efficient correlation approach have been proposed and implemented. A linear strain response down to 47.5 pε and a strain resolution up to 0.1 nε/sqrt(Hz) have been confirmed. The high linearity, high strain resolution and measurement repetition rate is achieved by physically substantiated optimization of the measurement parameters related to the correlation and interpolation approaches. A dynamic sweep range extension technique has been demonstrated which allows for theoretically unlimited continuous strain range measurement without the need for a tunable laser or filter. A significant advantage in comparison to other phase-resolved DVS approaches is that an interrupted strain measurement can be resumed without loss of the reference, if the strain range of the extended sweep range is not exceeded. The field applicability and the robust correlation performance have been demonstrated by means of distributed strain measurements and vibration mode analysis of a reinforced concrete bridge.

The experimental setup is fully compatible with single-wavelength DVS approaches and can also be used for conventional vibration sensing well into the MHz range. The bandwidth of the presented wavelength-scanning mode is reduced by the number of wavelengths that are used for the correlation. The achievable measurement repetition rate in the kHz-range for kilometer fiber lengths is more than sufficient for the intended applications.

The technique provides a potent new method for the structural monitoring applications and can, for instance, be used for distributed vibration analysis, localized damage assessment and remaining lifetime predictions of critical infrastructure. The high spatial resolution down to the sub-meter range is a prerequisite to clearly separating mode parameters and reliably detecting and monitoring structural discontinuities and damages, such as material fatigue and sub- μm crack propagation. The extremely high strain resolution makes it possible to conduct distributed ambient vibration analysis. Also the geophysical sector is a potential field of application, for example for active and passive seismic applications or ambient noise tomography.

Funding

BAM Themenfeld Projekt “Bewertung, Lebensdauerprognose und Instandsetzung von Brückenbauwerken” (BLEIB).

Acknowledgment

We thank the project leader Jörg Unger and all other partners involved in the project.